








CrossMark

Formation of Phosphorus Monoxide (PO) in the Interstellar Medium: Insights from Quantum-chemical and Kinetic Calculations

Juan García de la Concepción¹ , Cristina Puzzarini² , Vincenzo Barone³ , Izaskun Jiménez-Serra¹ , and Octavio Roncero⁴ 

¹ Centro de Astrobiología (CSIC-INTA), Ctra. de Ajalvir Km. 4, Torrejón de Ardoz, E-28850 Madrid, Spain; jgarcia@cab.inta-csic.es

² Department of Chemistry “Giacomo Ciamician”, University of Bologna, Via F. Selmi 2, Bologna, I-40126, Italy; cristina.puzzarini@unibo.it

³ Scuola Normale Superiore, Piazza dei Cavalieri 7, Pisa, I-56126, Italy; vincenzo.barone@sns.it

⁴ Instituto de Física Fundamental (IFF), C.S.I.C., Serrano 123, E-28006 Madrid, Spain

Received 2021 June 25; revised 2021 August 12; accepted 2021 August 16; published 2021 November 29

Abstract

In recent years, phosphorus monoxide (PO), an important molecule for prebiotic chemistry, has been detected in star-forming regions and in the comet 67P/Churyumov-Gerasimenko. These studies have revealed that, in the interstellar medium (ISM), PO is systematically the most abundant P-bearing species, with abundances that are about one to three times greater than those derived for phosphorus nitride (PN), the second-most abundant P-containing molecule. The reason why PO is more abundant than PN remains still unclear. Experimental studies with phosphorus in the gas phase are not available, probably because of the difficulties in dealing with its compounds. Therefore, the reactivity of atomic phosphorus needs to be investigated using reliable computational tools. To this end, state-of-the-art quantum-chemical computations have been employed to evaluate accurate reaction rates and branching ratios for the $P + OH \rightarrow PO + H$ and $P + H_2O \rightarrow PO + H_2$ reactions in the framework of a master equation approach based on ab initio transition state theory. The hypothesis that OH and H₂O can be potential oxidizing agents of atomic phosphorus is based on the ubiquitous presence of H₂O in the ISM. Its destruction then produces OH, which is another very abundant species. While the reaction of atomic phosphorus in its ground state with water is not a relevant source of PO because of emerged energy barriers, the $P + OH$ reaction represents an important formation route of PO in the ISM. Our kinetic results show that this reaction follows an Arrhenius–Kooij behavior, and thus its rate coefficients ($\alpha = 2.28 \times 10^{-10} \text{ cm}^3 \text{ molecule}^{-1} \text{ s}^{-1}$, $\beta = 0.16$ and $\gamma = 0.37 \text{ K}$) increase by increasing the temperature.

Unified Astronomy Thesaurus concepts: [Interstellar molecules \(849\)](#); [Chemical abundances \(224\)](#); [Reaction rates \(2081\)](#)

1. Introduction

Phosphorus (P) is a key element for life, indeed being present in all living systems (Gulick 1957; Maciá 2005; Schwartz 2006; Fernández-García et al. 2017). It is an essential constituent of biomolecules, where it plays a key role in crucial processes such as information transfer and replication (RNA and DNA), formation of cellular membranes (phospholipids), and energy production in living cells (ATP).

Compared to living systems ($P/H = 10^{-3}$, Fagerbakke et al. 1996), the abundance of P (with respect to hydrogen) in the Universe is low ($P/H = 2.8 \times 10^{-7}$; Grevesse & Sauval 1998). P is known to form in massive stars and it is distributed throughout the interstellar medium (ISM) by supernova explosions (Koo et al. 2013). It is believed that P became available in the early Earth during the Late Heavy Bombardment period, i.e., between 4.1 to 3.8 billion years ago, when this element was delivered by the impact of small bodies such as meteorites (Pasek & Lauretta 2005) and comets similar to Halley and 67P/Churyumov-Gerasimenko (67P/C-G; Altwegg et al. 2016).

Phosphates PO_4^{2-} , and their derivatives, are the source of P in biomolecules. Thus, from a chemical point of view, the oxidized forms of P are of particular interest. Among oxygenated P-bearing species, phosphorus monoxide (PO) is the simplest molecule, and it can be seen as the building block of small biomolecules (Douglas et al. 2020). PO has already been detected in different circumstellar environments and star-forming regions, where several observational studies have systematically pointed out that PO is more abundant than PN (the second-most

abundant P-bearing species detected in molecular clouds) by a factor of about one to three (Lefloch et al. 2016; Rivilla et al. 2016, 2018; Bergner et al. 2019; Rivilla et al. 2020; Bernal et al. 2021). Recently, Rivilla et al. (2020) have shown that PO, and not atomic phosphorus, is the reservoir of P in comet 67P/C-G.

Several mechanisms have been proposed to explain the production of P-bearing species in the ISM such as shock-induced formation (Yamaguchi et al. 2011; Aota & Aikawa 2012; Lefloch et al. 2016; Mininni et al. 2018; Rivilla et al. 2018), gas-phase reactions in the cold collapse phase (Rivilla et al. 2016) and gas-phase processes at high temperatures in massive hot cores (Charnley & Millar 1994). However, the question why PO is more abundant than PN in the gas phase is still open (Bergner et al. 2019; Bernal et al. 2021). Jiménez-Serra et al. (2018) revisited the chemistry of phosphorus in the ISM under different conditions and accounting for energetic phenomena (protostellar heating, cosmic rays, UV-photon radiation, and shock waves) in order to derive the PO/PN abundance ratio and understand how this is affected by different environments. To reproduce the PO/PN abundance ratios obtained in the molecular outflows of shocked regions (e.g., Yamaguchi et al. 2011; Lefloch et al. 2016), the gas-phase reaction between P and the OH radical was incorporated in the chemical network (Jiménez-Serra et al. 2018). However, the lack of kinetic information for such a reaction compelled the authors to assume that the rate constant is equal to that of the association reaction between N and OH yielding $NO + H$ (see Table 4 in Jiménez-Serra et al. 2018). Indeed, $N + OH$ is the main formation route of NO in star-forming regions and it is able to explain the NO abundances measured in protostellar envelopes and shocks (Codella et al. 2018).

At variance with N, the reactivity of atomic phosphorus with O-bearing species such as OH and water, but also atomic O, has so far only marginally been studied. The radiative association between P and O to produce PO in its doublet ground state, has been investigated by Andreatza et al. (2016). Their quantum-chemical calculations show that this reaction is inefficient in the ISM because the derived rate constants are too small; indeed, in the range between 300 and 14,000 K, they vary from 1.6×10^{-24} to $2.0 \times 10^{-18} \text{ cm}^3 \text{ molecule}^{-1} \text{ s}^{-1}$ (Andreatza et al. 2016). The reaction of atomic phosphorus (4S and 2D) with molecular oxygen, O_2 , has been studied from both experimental and theoretical points of view (Douglas et al. 2019). However, several discrepancies have been found in the kinetics of the reaction between P in its ground state (4S) and O_2 , which seems to show an unusual temperature dependence (Husain & Norris 1977; Husain & Slater 1978; Clyne & Ono 1982; Henshaw et al. 1987; Douglas et al. 2019). Finally, to the best of our knowledge, the gas-phase $P + OH \rightarrow PO + H$ and $P + H_2O \rightarrow PO + H_2$ reactions have not yet been investigated neither experimentally nor theoretically.

In this paper, we report the main results of a comprehensive computational study on the formation of phosphorus monoxide ($^2\Pi$) from the reactions of atomic P with the hydroxyl radical (OH) and with water (H_2O). Although atomic phosphorus in the ISM should be in the electronic ground state 4S , we have also considered its metastable (first) excited state 2D because its formation is associated with high energetic processes (Koo et al. 2013). As potential oxidizing agents of atomic phosphorus, H_2O and OH have been employed. The former species is highly abundant in the ISM and is destroyed through different mechanisms to yield OH (Tappe et al. 2008; Viti et al. 2011). The paper is organized as follows. Section 2 describes the computational methodology. Section 3 presents the results on the potential energy profiles and kinetics for both the reactions considered. In Section 4, we discuss the astrophysical implications and, finally, in Section 5, we summarize our conclusions.

2. Computational Methodology

The starting point for the study of the formation pathways of 2PO is the identification of the potential reactants and the analysis of the corresponding reactive potential energy surface (PES) to accurately characterize all stationary points from both a structural and energetic point of view. In a second step, kinetic calculations are performed under the very low temperatures (10–100 K) and pressures ($10\text{--}10^7 \text{ cm}^{-3}$ in terms of number density) typical of the ISM.

2.1. Reactive Potential Energy Surface

To characterize the reactive PES, we have followed a well-established computational strategy (Vazart et al. 2016; Lupi et al. 2020; Puzzarini et al. 2020) that has recently been employed in the investigation of the formation mechanisms of different interstellar molecules (Baiano et al. 2020; Lupi et al. 2020; Puzzarini et al. 2020; Tonolo et al. 2020; Alessandrini et al. 2021). This strategy consists of the following steps.

First, all stationary points of the reactive PES have been located and characterized using the double-hybrid revDSD-PBEP86 functional (Kozuch & Martin 2011; Santra et al. 2019) combined with the D3(BJ) corrections to incorporate dispersion effects (Grimme et al. 2010, 2011). This functional has been used in conjunction with the jun-cc-pVTZ basis set, thereby

using the set with an additional d function on P, jun-cc-pV(T+d)Z (Dunning et al. 2001; Papajak et al. 2009; Prascher et al. 2011). In the following, this level of computation will be simply referred to as revDSD. The nature of the stationary points located on the PES has been confirmed by Hessian evaluations at the same level of theory, which also provide the corresponding harmonic zero-point vibrational energy (ZPE) corrections. To ensure the right connection between transition states and minima, intrinsic reaction coordinate analyses have been performed throughout the PESs characterization (Crehuet & Bofill 2005). To further check the reliability of the revDSD structural characterizations, for the reaction involving the OH radical, the stationary points of the reactive PES have also been optimized using the explicitly correlated CCSD(T)-F12b method (Adler et al. 2007; Knizia et al. 2009; Werner et al. 2011) in conjunction with the cc-pVTZ-F12 basis set (Peterson et al. 2008), within the frozen-core (fc) approximation. Furthermore, we compared our results with those available in the literature for the HOP and HPO species (Francisco 2003; Puzzarini 2006). In passing, we note that revDSD geometries well agree with those obtained using different coupled-cluster formulations.

In a second step, single-point energy calculations, on top of revDSD geometries, have been performed by means of the composite scheme denoted as HEAT-like because based on the HEAT protocol (Tajti et al. 2004; Bomble et al. 2006; Harding et al. 2008). As detailed in Puzzarini & Barone (2020), Lupi et al. (2020), Puzzarini et al. (2020), the HEAT-like scheme relies on the additivity approximation, with the different contributions required for obtaining highly accurate results evaluated at the best possible level and then combined together:

$$E_{\text{tot}} = E_{\text{HF-SCF}}^{\infty} + \Delta E_{\text{CCSD(T)}}^{\infty} + \Delta E_{\text{CV}} + \Delta E_{\text{fT}} + \Delta E_{\text{fQ}} + \Delta E_{\text{REL}} + \Delta E_{\text{DBOC}}. \quad (1)$$

In the expression above, $E_{\text{HF-SCF}}^{\infty}$ and $\Delta E_{\text{CCSD(T)}}^{\infty}$ denote the extrapolation to the complete basis set (CBS) limit of the HF-SCF energy using the exponential formula by Feller (1993) and the CCSD(T) correlation energy (within the fc approximation) extrapolated to the CBS limit with the n^{-3} expression (Helgaker et al. 1997), respectively. The correlation-consistent cc-pVnZ basis sets (Dunning 1989) have been employed in conjunction with these calculations, with $n = Q, 5$, and 6 being chosen for the HF-SCF extrapolation, and $n = Q$ and 5 for the CCSD(T) correlation energy. The ΔE_{CV} term allows for incorporating the core-valence correlation correction, evaluated as energy difference between all-electron (ae) and fc-CCSD(T) computations in the same basis, which is, in the present case, the cc-pCVQZ set (Woon & Dunning 1995; Peterson & Dunning 2002). In a similar manner, corrections due to the full treatment of triple, ΔE_{fT} , and quadruple, ΔE_{fQ} , excitations are computed as energy differences between CCSDT (Noga & Bartlett 1987; Scuseria & Schaefer 1988; Watts & Bartlett 1990) and CCSD(T) and between CCSDTQ (Kállay & Surján 2001) and CCSDT (all within the fc approximation) employing the cc-pVTZ and cc-pVDZ basis sets, respectively. The diagonal Born–Oppenheimer correction (Sellers & Pulay 1984; Handy et al. 1986; Handy & Lee 1996; Kutzelnigg 1997), ΔE_{DBOC} , and the scalar relativistic contribution (Cowan & Griffin 1976; Martin 1983), ΔE_{REL} , to the energy, are also included. The former correction has been computed at the HF-SCF/aug-cc-pVTZ level (Kendall et al. 1992), whereas the relativistic corrections have been obtained at the ae-CCSD(T)/aug-cc-pCVTZ level including the (one-electron) Darwin and mass-

velocity terms. Incorporation of CCSDTQ computations in the composite scheme should account for non-dynamical electron correlation effects; to further check this point, for the stationary points showing a multi-reference character (deduced from the value of the T_1 diagnostic; Lee & Taylor 1989), the correction due to pentuple excitations has also been considered and incorporated as energy difference between CCSDTQP (Kállay & Surján 2001) and CCSDTQ computations carried out within the fc approximation and in conjunction with the cc-pVDZ basis set. Finally, HEAT-like energies have been augmented by anharmonic ZPE corrections evaluated at the revDSD level within vibrational perturbative theory to second order (VPT2; Barone 2004).

The conclusive test on the reliability of coupled-cluster calculations has been provided by multiconfigurational computations using the n -electron valence state perturbation theory (NEVPT2) method (Angeli et al. 2001a, 2001b). This has been employed in conjunction with the minimally augmented ma-def2-(T+d)ZVP basis set. The active space chosen for the phosphorus atom is three electrons in 3 p atomic orbitals (3,3). For the OH radical, a (5,4) active space (i.e., the two $p\pi$ orbitals and the pair $p\sigma$ and $p\sigma^*$) has been selected instead. The overall active space employed is (8,7). Since the NEVPT2 test for the stationary points showing relevant non-dynamical correlation effects conclusively demonstrated the reliability of our coupled-cluster approach, we will not mention further NEVPT2 results.

All DFT and VPT2 calculations have been carried out with the Gaussian software (Frisch et al. 2016), while those for the HEAT-like scheme have been performed using the CFOUR program (Stanton et al. 2016; Matthews et al. 2020), except those including quadruple and quintuple excitations (CCSDTQ, CCSDTQP) which have been performed with the MRCC code (Kállay et al. 2018) interfaced to CFOUR. NEVPT2 computations have been carried out with the ORCA software (Neese et al. 2020), while explicitly correlated CCSD(T)-F12b calculations have been performed using the MOLPRO software (Werner et al. 2019).

2.2. Kinetic Calculations

For elementary steps ruled by well-defined saddle points, the unimolecular rate coefficients were calculated using Rice–Ramsperger–Kassel–Marcus theory within the rigid-rotor harmonic-oscillator approximation (Weston & Schwartz 1972). Barrierless bimolecular association rate constants were instead obtained employing the phase space theory (PST; Pechukas & Light 1965; Chesnavich 1986), where the attractive potential between the two fragments at large distances is described by a $V_{\text{MEP}} = \frac{-C}{R^6}$ functional form with the C constant derived from a fit of the revDSD energies. The C values obtained for the barrierless processes are gathered in Table 1. Semiclassical one-dimensional tunneling corrections were evaluated using the Eckart model (Eckart 1930). Subsequently, the temperature and pressure-dependent phenomenological rate coefficients have been calculated by using a master equation approach based on transition state theory (AITSTME), employing the MESS software as master equation solver (Georgievskii et al. 2013), which is available at <https://github.com/PACChem/MESS>. The input information for MESS can be provided upon request.

The global rate coefficients have been computed in the 30–400 K range, and to describe its temperature dependence, a modified Arrhenius expression, the Arrhenius–Kooij formula

Table 1
C Coefficients for PST Calculations (in Hartree/bohr⁶) of the Barrierless Processes

Reaction	Coefficient
$^4\text{P} + ^2\text{OH} \rightarrow ^3\text{POH}$	112.479
$^3\text{HPO} \rightarrow ^2\text{PO} + ^2\text{H}$	26.886
$^4\text{P} + \text{H}_2\text{O} \rightarrow ^4\text{C_P-OH2}$	112.067
$^2\text{P} + \text{H}_2\text{O} \rightarrow ^2\text{C_P-OH2}$	905.650

(Kooij 1893), has been used:

$$k(T) = \alpha \left(\frac{T}{300} \right)^\beta \exp \left(-\frac{\gamma}{T} \right) \quad (2)$$

where α , β , and γ are fitting parameters, determined using the computed rate coefficients at different temperatures.

3. Results

In the following, the reactive PESs of the P + OH and P + H₂O reactions and their thermochemistry are described in detail, then the kinetics of both reactions is addressed.

3.1. Reaction of P(⁴S) and P(²P) with Hydroxyl Radical (OH, ²II)

Figure 1 shows the HEAT-like potential energy profiles (with anharmonic ZPE corrections) for the proposed mechanisms of the reaction of atomic phosphorus with the hydroxyl radical. There are two entrance channels, one for each multiplicity, which lead to the pre-reactive complexes ¹POH and ³POH. In the triplet PES, the formation of ³POH is barrierless, whereas the formation of ¹POH proceeds through a transition state, ¹TS_P-OH. Therefore, only the formation of ³POH is a viable option. Indeed, to form ¹POH, the system has to overcome an energy barrier of 85.0 kJ mol⁻¹. In the ISM, because of the very low temperature, only reactions with submerged barriers can occur.

From the pre-reactive complexes, ³POH and ¹POH, the PESs bifurcates into two pathways. The first exit channel leads to ²PO + ²H through the transition structures ³TS_PO-H and ¹TS_PO-H, which correspond to the dissociation of the O-H bond. The energy difference between these saddle points is small (18.1 kJ mol⁻¹). However, the energy barrier ruling the ³POH dissociation is 227.3 kJ mol⁻¹, which is reduced to 181.0 kJ mol⁻¹ for ¹POH. This difference in the barriers is mainly due to the fact that ³POH lies 64.4 kJ mol⁻¹ below ¹POH. Although the barrier for the triplet PES is higher than that for the singlet, this can be easily overcome because the system accumulates the energy of the reactants, which cannot be dissipated by third-body collisions due to the very low pressures of the ISM.

The second pathway proceeds with the isomerization of the pre-reactive complexes to ³HPO and ¹HPO for the triplet and singlet PES, respectively. The energy difference between the corresponding transition states, ³TS_POH-HPO and ¹TS_POH-HPO, is again small (16.7 kJ mol⁻¹), but the energy barriers differ considerably because of the relative stability of ³POH and ¹POH. These are 174.2 kJ mol⁻¹ and 126.5 kJ mol⁻¹ for the triplet and singlet PES, respectively. The PESs for the hydrogen migration are very different for the two spin states: the isomerization of ¹POH to ¹HPO is exothermic (−144.0 kJ mol⁻¹), whereas from ³POH to

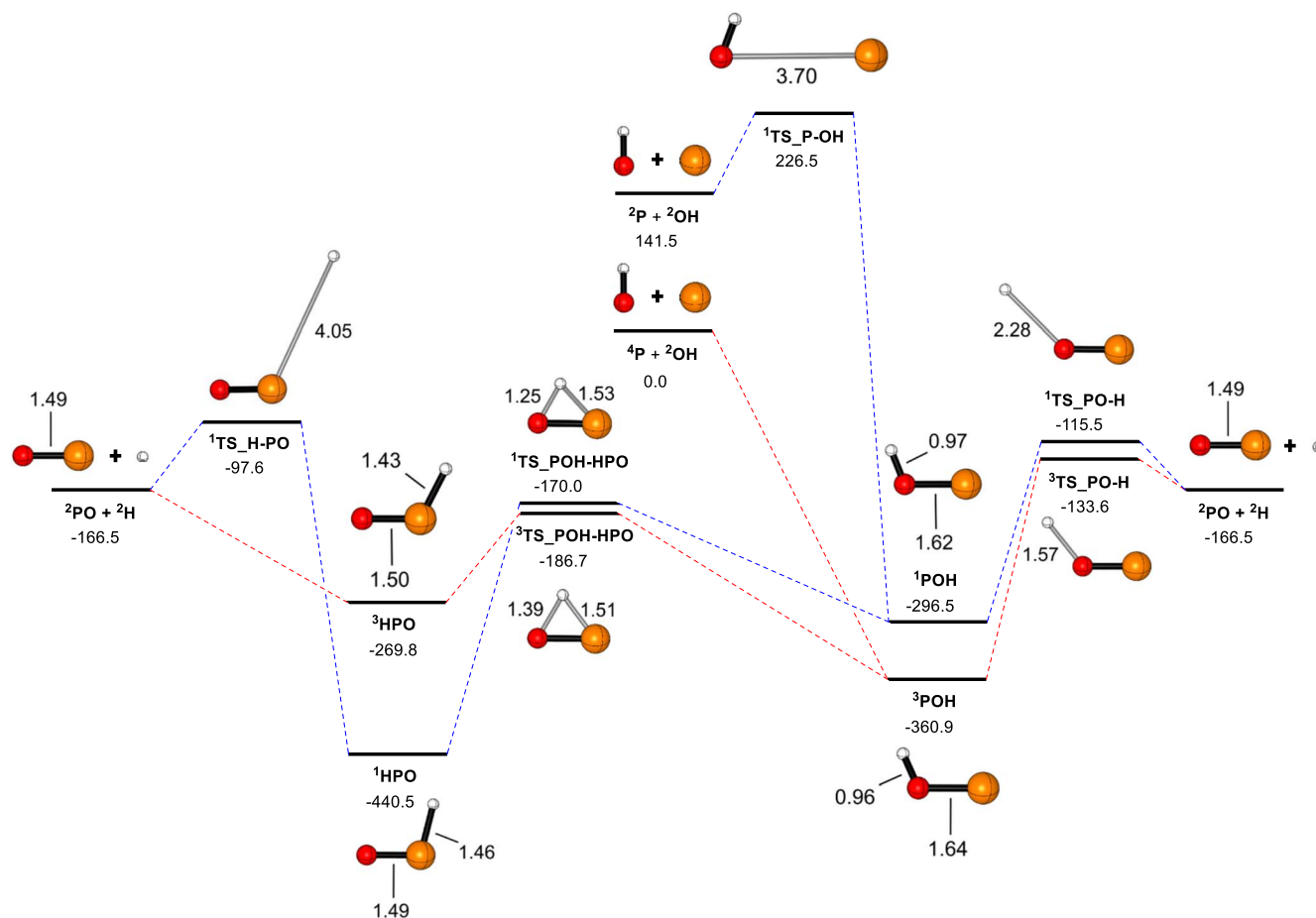


Figure 1. Singlet (blue profile) and triplet (red profile) potential energy surfaces (ZPE-corrected energies) for the formation of PO from OH + P.

^3HPO the process is endothermic (91.1 kJ mol^{-1}). These findings are in good agreement with those reported in Francisco (2003).

The last part of the mechanism is the dissociation of the P-H bond in the intermediates ^3HPO and ^1HPO , which is the second exit channel. While in the triplet PES the process is barrierless, in the singlet PES, the dissociation of the P-H in ^1HPO goes through a high energy barrier ($342.9 \text{ kJ mol}^{-1}$), ruled by the $^1\text{TS}_{\text{H-PO}}$ transition state. We have also considered the dissociation of ^3HPO to $^1\text{PH} + \text{O}(^3\text{P})$, and of ^1POH to $^1\text{PH} + \text{O}(^1\text{D})$ and $^3\text{PH} + \text{O}(^3\text{P})$. However, these dissociation paths are endothermic processes (revDSD energies are given in Table 2), which are thus not viable in the extreme conditions of the ISM. Therefore, they have not been further investigated.

Overall, we can conclude that, from a thermochemical point of view, the formation of ^2PO from the reaction between ^2OH and $\text{P}(^4\text{S})$ is feasible, the rate-determining step of the whole process being the barrierless association between the reactants. On the other hand, the formation of ^2PO on the singlet PES is unlikely, since the rate-determining step is the formation of ^1POH , which is ruled by a non-negligible energy barrier. The energy profile depicted in Figure 1 shows some regions where the two PESs could cross through minimum energy crossing points. These are the first exit channel and the isomerizations of ^3POH and ^1POH . However, as mentioned above, the most relevant parts of the whole processes are the association reactions to yield the intermediates ^3POH and ^1POH . In these first steps, the potential energies of the two PESs are well separated and they cannot cross. In addition, the energy of the

reactants is very high in comparison with the rest of the stationary points. Therefore, crossings in the pathways, if any, are not expected to influence the kinetics of the reaction.

The relative energies of the paths discussed above are collected in Table 2, where the results for revDSD and the HEAT-like composite scheme are compared. Such a comparison shows average deviations of $10\text{--}15 \text{ kJ mol}^{-1}$, thus suggesting that revDSD is suitable for semiquantitative investigations. The HEAT-like data augmented for ZPE corrections evaluated at an anharmonic level are also provided. A note on the pentuples correction is also deserved. Their contribution to relative energies is smaller than 1 kJ mol^{-1} even for the species showing the largest multi-reference character, thus supporting the conclusion that the full treatment of quadruple excitations is already able to incorporate non-dynamical correlation in the energy determination.

3.2. Reaction of $\text{P}(^4\text{S})$ and $\text{P}(^2\text{P})$ with Water (H_2O)

The reactivity of atomic phosphorus with H_2O is very different with respect to that with OH. First of all, the high-spin (quartet) PES corresponding to the reaction between H_2O and $\text{P}(^4\text{S})$ is not expected to proceed toward the desired product, i.e., PO, under the conditions of the ISM. In fact, after the barrierless formation of a van der Waals pre-reactive complex ($^4\text{C}_{\text{P-OH}_2}$), whose relative energy is only $\sim 1 \text{ kJ mol}^{-1}$ below the reactants, the process toward the triplet ^3POH and atomic hydrogen (^2H) goes through a transition state $^4\text{TS}_{\text{P-OH}_2}$ (with a barrier of $213.3 \text{ kJ mol}^{-1}$). According to the discussion in the previous section (see also Figure 1), two possible reaction

Table 2
Relative Energies (in kJ mol^{-1}) for the $\text{P}(^4S)/\text{P}(^2P) + \text{OH}(^2\Pi)$ Reaction

	revDSD ^a	HEAT-like ^b	HEAT-like + ZPE _{anh} ^c
Triplet PES			
$^4\text{P} + ^2\text{OH}$	0.0	0.0	0.0
^3POH	-364.0	-371.5	-360.9
$^3\text{TS}_{\text{PO-H}}$	-105.3	-120.0	-133.6
$^3\text{TS}_{\text{POH-HPO}}$	-166.4	-182.5	-186.7
^3HPO	-262.1	-272.5	-269.8
$^2\text{PO} + ^2\text{H}$	-144.8	-151.5	-166.5
$^1\text{PH} + \text{O}(^3P)$	267.3
Singlet PES^d			
$^2\text{P} + ^2\text{OH}$	175.4	141.5	141.5
$^1\text{TS}_{\text{P-OH}}$	209.0	225.7	226.5 (225.8)
^1POH	-287.7	-308.0	-296.5
$^1\text{TS}_{\text{PO-H}}$	-57.5	-102.7	-115.5 (-116.6)
$^1\text{TS}_{\text{POH-HPO}}$	-151.3	-166.0	-170.0
^1HPO	-432.9	-444.1	-440.5
$^1\text{TS}_{\text{H-PO}}$	-59.8	-82.0	-97.6 (-98.3)
$^2\text{PO} + ^2\text{H}$	-144.8	-151.5	-166.5
$^1\text{PH} + \text{O}(^1D)$	343.5
$^3\text{PH} + \text{O}(^1P)$	133.7

Notes.^a revDSD-PBEP86-D3(BJ)/jun-cc-pV(T+d)Z; see text.^b CCSD(T)/CBS+CV+DBOC+Rel+fT+fQ; see text.^c CCSD(T)/CBS+CV+DBOC+Rel+fT+fQ+ZPE_{anh}; CCSD(T)/CBS+CV+DBOC+Rel+fT+fQ+fP+ZPE_{anh} results given within parentheses; see text.^d Referred to $^4\text{P} + ^2\text{OH}$.

pathways are available from ^3POH to $^2\text{PO} + ^2\text{H}$. However, both of them are ruled by non-negligible energy barriers. The path from $\text{H}_2\text{O} + \text{P}(^4S)$ to $^3\text{POH} + \text{H}$ is depicted in Figure 2 (red profile).

From a chemical point of view, the reaction between H_2O and $\text{P}(^2P)$ is instead expected to occur in the ISM. However, it requires the presence of atomic phosphorus in an excited electronic state, whose abundance should be negligible in the ISM with respect to that of the ground state. The reaction mechanism starts with the formation of the pre-reactive complex $^2\text{C}_{\text{P-OH}_2}$ (47.2 kJ mol^{-1} below the reactants, 94.0 kJ mol^{-1} above the reactants in the quartet state), which evolves to $^2\text{PHOH-anti}$ by overcoming the transition state $^2\text{TS}_{\text{P-OH}_2}$ (with a barrier of 22.6 kJ mol^{-1}), which lies 24.6 kJ mol^{-1} below the reactants of the doublet PES. Then, $^2\text{PHOH-anti}$ can isomerize to $^2\text{PHOH-syn}$ (nearly isoenergetic with anti once ZPE is incorporated) by overcoming a small torsional barrier (18.3 kJ mol^{-1} , with $^2\text{TS}_{\text{PHOH-rot}}$ lying 12.5 kJ mol^{-1} below the doublet reactants). The exit channel is the loss of molecular hydrogen from $^2\text{PHOH-syn}$ to give $^2\text{PO} + \text{H}_2$ and it is characterized by a relatively high barrier ($^2\text{TS}_{\text{PO-H}_2}$) of about 251 kJ mol^{-1} . The path from $\text{H}_2\text{O} + \text{P}(^4S)$ to $\text{PO} + \text{H}_2$ is depicted in Figure 2 (blue profile). As noted for the reaction of $^2\text{OH} + \text{P}(^4S)$, the rate-determining step of this mechanism is the barrierless association between the reactants. In passing, we note that the dissociation of either $^2\text{PHOH-syn}$ or $^2\text{PHOH-anti}$ to $^1\text{PH} + ^2\text{OH}$ has been investigated. As noted for the $\text{P} + \text{OH}$ reaction, the formation of PH is an endothermic process (revDSD energies are available in Table 3). Therefore, it has not been further considered.

In analogy with the $\text{P} + \text{OH}$ reaction, we collect and compare in Table 3 the relative revDSD and HEAT-like energies of the paths discussed above. The comparison shows a better agreement between revDSD and HEAT-like results with

respect to the $\text{P} + \text{OH}$ reaction, with an average deviation of the order of a few kJ mol^{-1} . The better agreement is probably due to the fact that, for the reaction under consideration, the T_1 diagnostics did not point out any multi-reference character. In Table 3, the HEAT-like values corrected for the ZPE contribution evaluated at an anharmonic level are also listed.

3.3. Kinetics

While thermochemistry provides hints on the viability of the studied reactions, to quantitatively understand whether they reasonably proceed toward the desired products, global rate constants need to be calculated. As described in the methodology section, we have resolved the one-dimensional master equation in the 30–400 K temperature range and at pressures of 10^{-7} atm. Figure 3 shows the plots of the bimolecular rate constants as a function of the temperature for the four reaction channels studied. Panels (a) and (b) refer to the reactions of ^4P and ^2P with ^2OH , respectively, whereas panels (c) and (d) refer to the reactions of ^4P and ^2P with H_2O , respectively. In addition, for the four reactions, Tables 4 and 5 report the global rate constants in the temperature range considered and the resulting parameters of the Arrhenius–Kooij equation, respectively.

As mentioned in Section 3.1, the rate-determining step for the reaction of ^2OH with both ^2P and ^4P is the formation of the POH adduct, with all the other reaction steps being characterized by submerged barriers. The entrance channel of the singlet PES shows a transition state ($^1\text{TS}_{\text{P-OH}}$) that lies at 85.0 kJ mol^{-1} above the reactants in the doublet state. This makes the reaction very slow, as demonstrated by the extremely small global rate coefficients, which lie between 0.0 (at 30 K) and 5.39×10^{-22} (at 400 K) $\text{cm}^3 \text{ molecule}^{-1} \text{ s}^{-1}$. The temperature dependence is well reproduced by the Arrhenius–Kooij model (see Equation (2)), as can be seen in Figure 3, with fitting parameters $\alpha = 2.97 \times 10^{-11} \text{ cm}^3 \text{ molecule}^{-1} \text{ s}^{-1}$, $\beta = 1.11$ and $\gamma = 1.00 \times 10^4 \text{ K}$. We note a strong temperature dependence from 30 to 100 K (the curve being very steep), while above the latter temperature, the variation of the rate coefficient is less evident. A similar trend is also observed for the triplet PES, even if, in such a case, the temperature dependence is smoother in the entire range considered. Since the entrance channel of the $^4\text{P} + \text{OH}$ reaction is barrierless, the global rate coefficients are greater and range between 1.55×10^{-10} and 2.38×10^{-10} for temperatures between 30 and 400 K. These global rate coefficients indicate that this pathway to PO is very efficient at the temperatures typical of the ISM. The derived α , β , and γ fitting parameters are $2.28 \times 10^{-10} \text{ cm}^3 \text{ molecule}^{-1} \text{ s}^{-1}$, 0.16, and 0.37 K, respectively. Finally, from the inspection of Figure 1, we note that the backward reactions are not feasible from any intermediate because the reactants are much higher in energy than any other minimum.

Moving to the reaction with water, we note that, when considering the high-spin atomic phosphorus (^4P), the formation of the intermediate $^3\text{POH} + \text{H}$ is not feasible at low temperature because of the high energy of the transition state $^4\text{TS}_{\text{PO-H}_2}$ (see Section 3.2). This reaction also shows an Arrhenius behavior similar to that of $^2\text{P} + \text{OH}$, with the rate coefficients increasing by increasing the temperature, although the rate coefficients remain extremely small. Indeed, they range from 0.0 at 30 K to $6.31 \times 10^{-39} \text{ cm}^3 \text{ molecule}^{-1} \text{ s}^{-1}$ at 400 K (see Table 4). These low rate constants are well reproduced by the α , β , and γ parameters of the Arrhenius–Kooij expression, these being $3.00 \times 10^{-25} \text{ cm}^3 \text{ molecule}^{-1} \text{ s}^{-1}$, 14.87 and $1.48 \times 10^4 \text{ K}$. Contrary to the reaction with OH, the association between the first metastable excited state

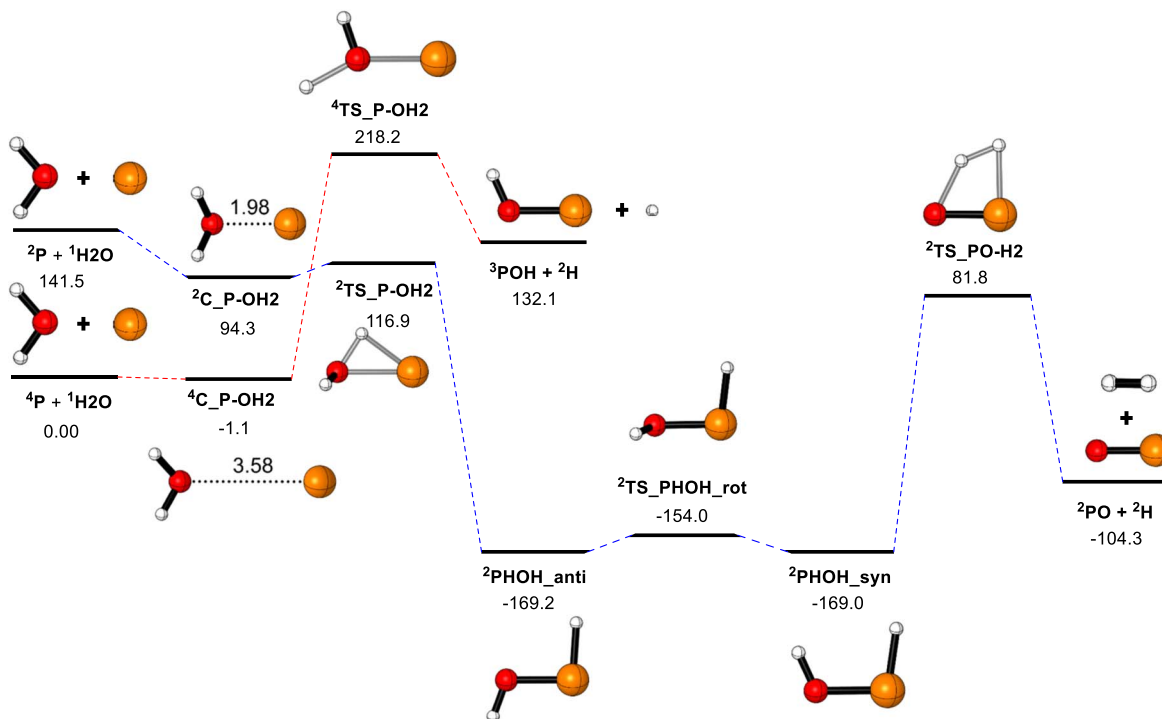


Figure 2. Doublet (blue profile) and quartet (red profile) potential energy surfaces (ZPE-corrected energies) for the formation of PO from $\text{H}_2\text{O} + \text{P}$.

Table 3
Relative Energies (in kJ mol^{-1}) for the $\text{P}(^4S)/\text{P}(^2P) + \text{H}_2\text{O}$ Reaction

	revDSD ^a	HEAT-like ^b	HEAT-like + ZPE _{anh} ^c
Quartet PES			
$^4\text{P} + \text{H}_2\text{O}$	0.0	0.0	0.0
$^4\text{C}_\text{P-OH2}$	-2.0	-1.7	-1.1
$^4\text{TS}_\text{P-OH2}$	231.4	237.7	218.2
$^3\text{POH} + ^2\text{H}$	149.8	154.8	132.1
Doublet PES^d			
$^2\text{P} + \text{H}_2\text{O}$	173.7	141.5	141.5
$^2\text{C}_\text{P-OH2}$	72.7	85.8	94.3
$^4\text{TS}_\text{P-OH2}$	125.8	123.6	116.9
$^2\text{PHOH}_\text{anti}$	-166.8	-168.7	-169.2
$^2\text{TS}_\text{PHOH}_\text{rot}$	-152.5	-150.9	-154.0
$^2\text{PHOH}_\text{syn}$	-170.9	-169.9	-169.0
$^2\text{TS}_\text{PO-H2}$	95.1	97.0	81.8
$^2\text{PO} + \text{H}_2$	-81.1	-82.2	-104.3
$^1\text{PH} + ^2\text{OH}$	206.5

Notes.

^a revDSD-PBEP86-D3(BJ)/jun-cc-pV(T+d)Z; see text.

^b CCSD(T)/CBS+CV+DBOC+Rel+fT+fQ; see text.

^c CCSD(T)/CBS+CV+DBOC+Rel+fT+fQ+ZPE_{anh}; see text.

^d Referred to $^4\text{P} + \text{H}_2\text{O}$.

of atomic phosphorus (^2P) and water presents a non-Arrhenius behavior from 70 K to higher temperatures (Figure 3(d)). This change in the temperature dependence is due to the fact that the pre-reactive complex and following transition state are very close in energy, and thus the actual temperature affects the easiness in overcoming the corresponding barrier. However, the rate-determining step of the whole process is the first barrierless association, and therefore this reaction channel is open at all temperatures here considered, with global rate coefficients ranging from 5.39×10^{-10} to $4.18 \times 10^{-10} \text{ cm}^3 \text{ molecule}^{-1} \text{ s}^{-1}$. The fitting parameters that

describe this temperature dependence of the rate constants are $\alpha = 5.88 \times 10^{-10} \text{ cm}^3 \text{ molecule}^{-1} \text{ s}^{-1}$, $\beta = 0.71$ and $\gamma = 51.47 \text{ K}$. For the reaction of water with ^2P , the reactants energy is well above all products and intermediates, and thus the reverse reaction can be considered not feasible. Indeed, the backward mechanism shows high energy transition states that cannot be overcome under typical ISM conditions.

4. Discussion

4.1. Comparison of the Rate Constants of the $\text{P} + \text{OH}$ and $\text{N} + \text{OH}$ Reactions

As mentioned in Section 1, the abundance of PO in the ISM is higher than that of PN in regions affected by shocks (either associated with molecular outflows or large-scale shocks in molecular clouds in the Galactic Center; see, e.g., Lefloch et al. 2016; Rivilla et al. 2016, 2018; Bergner et al. 2019). The observed abundance of PO with respect to PN is a useful indicator because it provides information about the length of the pre-stellar collapse phase (see Aota & Aikawa 2012; Lefloch et al. 2016). However, the lack of well-validated kinetic data for the formation of PO hampers our understanding of the reason why PO consistently appears to be more abundant than PN in the ISM. Since the reaction kinetic information on $\text{P} + \text{OH} \rightarrow \text{PO} + \text{H}$ was missing prior to this work, in order to incorporate it in the modeling of phosphorus chemistry in the ISM, Jiménez-Serra et al. (2018) assumed a rate constant for the association of P and OH similar to that of the well-studied $\text{N}(^4S) + \text{OH}(^2\Pi)$ reaction (see Daranlot et al. 2011, and references therein). To check the validity of this assumption, we here compare the rate constant of the reaction $\text{N}(^4S) + \text{OH}(^2\Pi)$ with that calculated in Section 3.3 for the $\text{P} + \text{OH}$ reactive system.

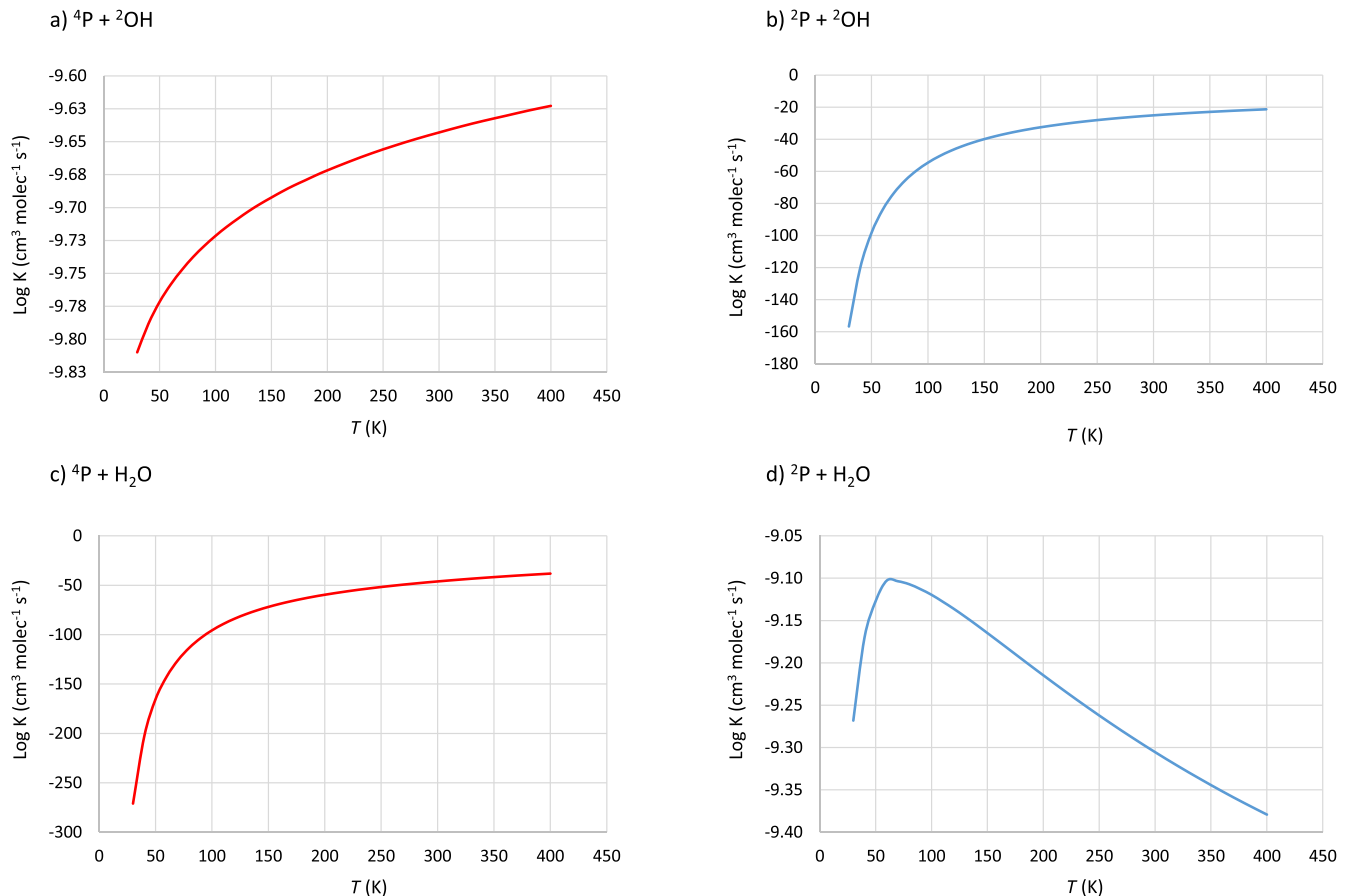


Figure 3. Plots of global rate coefficients (log scale) for the P+OH and P + H₂O reactions in the 30–400 K.

In Figure 4, we show the temperature dependence of the global rate constants for the reaction $\text{P}(^4S) + \text{OH}(^2\Pi) \rightarrow ^2\text{PO} + ^2\text{H}$ (red line; this work), and those available in the literature for the reaction $\text{N}(^4S) + \text{OH}(^2\Pi) \rightarrow \text{NO}(^2\Pi) + ^2\text{H}$. For the latter reaction, we compare the Arrhenius–Kooij fitting parameters provided by the UMIST (University of Manchester Institute of Science and Technology (McElroy et al. 2013); solid yellow line) and KIDA (KInetic Database for Astrochemistry (Wakelam et al. 2017); dotted yellow line) databases with the most recent experimental values for this reaction (Daranlot et al. 2011; black line). While the order of magnitude of the KIDA results is closer than the UMIST counterparts to the experimental values, the temperature dependence of the rate constant is better described by the UMIST data, which correctly reproduce the non-Arrhenius behavior observed in the experiment (in the ~ 80 – 300 K range). On the contrary, the global rate constant of the P + OH reaction shows an Arrhenius-like temperature dependence (see red line in Figure 4, and Section 3.3), and it is about one order of magnitude greater than that of the reaction between N and OH.

The explanation of the behaviors and results discussed above lies in the fact that $\text{P}(^4S)$ and $\text{N}(^4S)$ show very similar reaction mechanisms when they react with $\text{OH}(^2\Pi)$ (Li et al. 2011), but the exit channels present significant differences. While the exit channel yielding $\text{PO} + \text{H}$ from HPO is barrierless (see Figure 1), the dissociation of HNO leading to $\text{NO}(^2\Pi) + ^2\text{H}$ shows a transition state (see Figure 5 in Li et al. 2011), which is likely the cause of the non-Arrhenius behavior of the reaction $\text{N}(^4S) + \text{OH}(^2\Pi)$ at temperatures above 80 K. Furthermore, the

Table 4
Global Rate Constants (in $\text{cm}^3 \text{ molecule}^{-1} \text{ s}^{-1}$) evaluated at $1 \times 10^{-7} \text{ atm}^a$

T (K)	$^4\text{P} + ^2\text{OH}$	$^2\text{P} + ^2\text{OH}$	$^4\text{P} + \text{H}_2\text{O}$	$^2\text{P} + \text{H}_2\text{O}$
30	1.55E-10	0.00	0.00	5.39E-10
40	1.63E-10	0.00	0.00	6.76E-10
50	1.69E-10	4.01E-99	0.00	7.46E-10
60	1.74E-10	1.56E-84	0.00	7.89E-10
70	1.79E-10	4.21E-74	0.00	7.88E-10
80	1.83E-10	2.95E-66	0.00	7.81E-10
90	1.87E-10	3.58E-60	0.00	7.71E-10
100	1.90E-10	2.71E-55	2.24E-96	7.59E-10
110	1.93E-10	2.72E-51	5.75E-90	7.45E-10
120	1.96E-10	5.93E-48	1.34E-84	7.31E-10
130	1.98E-10	4.00E-45	4.96E-80	7.15E-10
140	2.01E-10	1.07E-42	4.32E-76	7.00E-10
150	2.03E-10	1.37E-40	1.18E-72	6.84E-10
160	2.05E-10	9.57E-39	1.27E-69	6.69E-10
170	2.07E-10	4.08E-37	6.35E-67	6.53E-10
180	2.09E-10	1.15E-35	1.67E-64	6.38E-10
190	2.11E-10	2.29E-34	2.57E-62	6.24E-10
200	2.13E-10	3.38E-33	2.51E-60	6.10E-10
220	2.16E-10	3.57E-31	7.86E-57	5.83E-10
240	2.19E-10	1.75E-29	7.69E-54	5.58E-10
260	2.22E-10	4.74E-28	3.10E-51	5.35E-10
280	2.25E-10	8.04E-27	6.28E-49	5.14E-10
300	2.27E-10	9.41E-26	7.35E-47	4.95E-10
320	2.30E-10	8.13E-25	5.51E-45	4.77E-10
340	2.32E-10	5.47E-24	2.85E-43	4.60E-10
360	2.34E-10	2.98E-23	1.06E-41	4.45E-10
380	2.36E-10	1.37E-22	2.95E-40	4.31E-10
400	2.38E-10	5.39E-22	6.31E-39	4.18E-10

Note.

^a All values lower than 1.0E-100 have been set equal to zero.

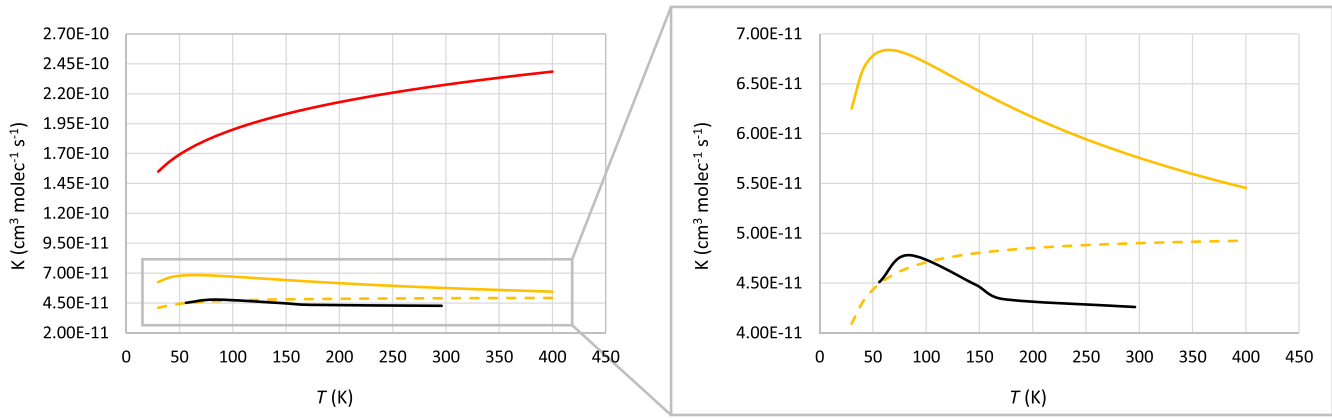


Figure 4. Plots of the temperature dependence of the global rate coefficients for the $P(^4S) + OH(^2\Pi)$ reaction (red line) compared with those, obtained from the Arrhenius–Kooij fitting parameters taken from UMIST (yellow solid line) and from KIDA (yellow dotted line), for the $N(^4S) + OH(^2\Pi)$ reaction. Experimental rate coefficients for the latter reaction (Daranlot et al. 2011) are also plotted (black line).

Table 5
Arrhenius–Kooij Parameters for the $P + OH$ and $P + H_2O$ Reactions

Fitting Parameters	$^4P + ^2OH$	$^2P + ^2OH$	$^4P + H_2O$	$^2P + H_2O$
$\alpha/cm^{-3} \text{ molecule}^{-1} s^{-1}$	2.28×10^{-10}	2.97×10^{-11}	3.00×10^{-25}	5.88×10^{-10}
β	0.16	1.11	14.87	-0.71
γ/K	0.37	1.00×10^4	1.48×10^4	51.47

presence of such a barrier in the exit channel for the $N + OH$ reaction might also explain the greater global rate constant when OH reacts with P. We can thus conclude that the $N(^4S) + OH(^2\Pi)$ reaction is not a good model for the $P(^4S) + OH(^2\Pi)$ reaction studied in this work, because the rate coefficients of the two reactions greatly differ in absolute value as well as in temperature dependence.

4.2. Astrophysical Implications for the $P + H_2O$ Reaction

Water is known to be ubiquitous in the ISM (van Dishoeck et al. 2021), and therefore it plays an important role in the oxidization of chemical species in the Universe. In the case of phosphorus, the oxidation reaction of P in its ground state (4S) with water to yield 2PO does not take place in the ISM, given its extremely low rate constant at all temperatures (see Table 4 as well as Figures 2 and 3(c)). However, the reaction of H_2O with the first excited state $P(^2P)$ is highly efficient (see Figure 3(d)), although most of the atomic phosphorus in the ISM should be in its ground state.

Water is also expected to be abundant in shocked regions associated with molecular outflows (Nisini et al. 2013; van Dishoeck et al. 2013, 2021; Suutarinen et al. 2014; Dionatos et al. 2020). However, even in regions with high abundances of water, the $P(^4S) + H_2O$ reaction is inefficient, the rate constant being $\sim 10^{-50} \text{ cm}^3 \text{ molecule}^{-1} \text{ s}^{-1}$ at temperatures in the 200–300 K range. This means that the formation of PO in the ISM through this chemical route is negligible. Water, however, can be either chemically destroyed at high temperatures (Viti et al. 2011) or UV-photon-dissociated by the radiative precursor of J -type shocks (Tappe et al. 2008), both processes yielding OH. Therefore, one can expect that the formation of PO through the $P + OH$ reaction becomes dominant in regions with large amounts of water, this latter acting as a precursor of OH. In the next section, this hypothesis will be investigated in further detail.

Table 6
Model Parameters Assumed for the L1157-B1 C -type Shock

Parameters	
$n(H)$	$2 \times 10^5 \text{ cm}^{-3}$
v_s	40 km s^{-1}
$T_{n,max}$	4000 K
B_0	$450 \mu\text{G}$
t_{sat}	4.6 yr

4.3. Chemical Modeling in a Shocked Region

In this section, we address the modeling of the phosphorus chemistry for an outflow shocked region with and without considering the PO formation routes explored in this work. As reference model, we will consider the C -type shock model that best reproduces the molecular abundances measured toward the B1 shocked region in the L1157 molecular outflow (see Viti et al. 2011; Holdship et al. 2016).

For the modeling of the phosphorus chemistry, we use the UCLCHEM chemical code (Holdship et al. 2017) and the phosphorus chemical network built by Jiménez-Serra et al. (2018). This chemical network is here updated by incorporating the rate constants of the $P(^4S) + OH(^2\Pi) \rightarrow ^2PO + ^2H$ and $P(^4S) + H_2O \rightarrow ^2PO + H_2$ processes (see Table 6). UCLCHEM is run in three phases: Phase 0 simulates the chemistry of a diffuse molecular cloud for 10^6 yr assuming an $n(H)$ density of 10^3 cm^{-3} and a temperature of 20 K. In Phase 1, the cloud undergoes free fall collapse at a constant temperature of 10 K until the final density of $2 \times 10^5 \text{ cm}^{-3}$ is reached. Finally, Phase 2 simulates the physical processes associated with the passage of a magneto-hydrodynamic (C -type) shock, which are commonly found in molecular outflows. For the physical structure of the C -type shock, we employ the same parameters used by Jiménez-Serra et al. (2008). Table 6 reports the input parameters of the L1157-B1 shock model, where $n(H)$ refers

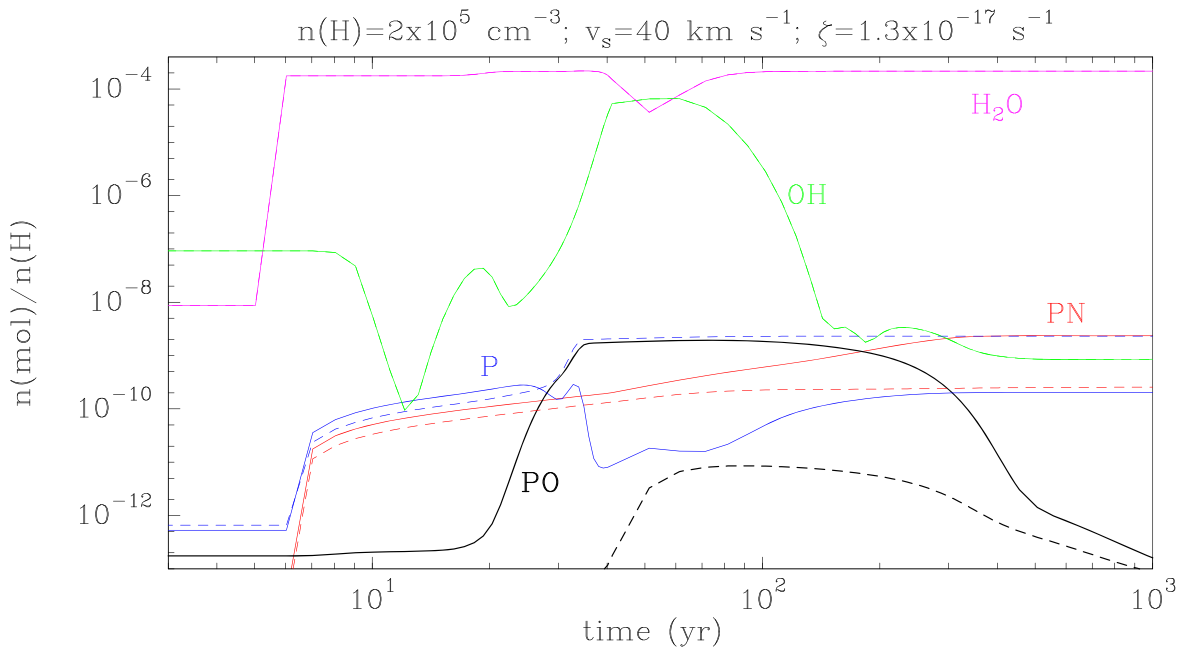


Figure 5. Abundances of P, PO, PN, OH, and H₂O predicted for Phase 2 of our model and assuming the shock parameters collected in Table 6. These shock parameters are those that best reproduce the molecular abundances measured in the L1157-B1 shocked region (Viti et al. 2011; Holdship et al. 2016). Solid lines refer to the results from the model *with* the new PO rate constants calculated in this work for the P + OH → PO + H and P + H₂O → PO + H₂ reactions. Dashed lines show the results for the model *without* the new rate constants for the formation of PO. The abundances of OH and H₂O are the same in both models.

to the initial volume density of the gas ($2 \times 10^5 \text{ cm}^{-3}$), v_s is the shock speed (40 km s^{-1}), $T_{n,\text{max}}$ is the maximum temperature achieved by the neutral gas in the post-shock region (4000 K), B_0 is the magnetic field strength ($450 \mu\text{G}$), and t_{sat} is the time at which the majority of the ice mantles of dust grains are released back into the gas phase due to sputtering (4.6 yr for an $n(\text{H})$ density of $2 \times 10^5 \text{ cm}^{-3}$; see Jiménez-Serra et al. 2018). For our shock model, we also consider a long-lived collapse of $6 \times 10^6 \text{ yr}$, i.e., once the final density is reached, it remains constant for about $7 \times 10^5 \text{ yr}$ longer. In addition, we assume a standard UV interstellar radiation field ($G_0 = 1$ in Draine units; see Viti & Williams 1999) and a standard cosmic-ray ionization rate ($\zeta = 1.3 \times 10^{-17} \text{ s}^{-1}$). The assumed initial abundance of P is 2.57×10^{-9} , as inferred by Aota & Aikawa (2012) and Lefloch et al. (2016) for the L1157-B1 shock.⁵ For further details on the modeling, the reader is referred to Jiménez-Serra et al. (2008).

In Figure 5, we present the results of the models of the phosphorus chemistry for the C-type shock parameters shown in Table 6. The abundances of the model *with* the new rate constants for the formation of PO, calculated in this work, are shown with solid lines, while the results from the model *without* these new rate constants are presented in dashed lines. The abundance of H₂O, P, and PN increase at the beginning of the shock (at about time 5 yr) due to the release of the icy mantles by the sputtering of dust grains (i.e., when time $\geq t_{\text{sat}}$; see Jiménez-Serra et al. 2018). The enhancement of P is tightly linked to the release of PH₃ from dust grains, since the latter is rapidly converted into PH₂, PH, and then P through the endothermic reactions $\text{PH}_3 + \text{H} \rightarrow \text{PH}_2 + \text{H}_2$, $\text{PH}_2 + \text{H} \rightarrow \text{PH} + \text{H}_2$ and $\text{PH} + \text{H} \rightarrow \text{P} + \text{H}_2$ (these reactions have

energy barriers from 318 to 735 K; see Charnley & Millar 1994).

The inclusion of the P + OH → PO + H and P + H₂O → PO + H₂ reactions in the chemical network does not modify noticeably the abundance of P and PN in the collapse phase, as shown by the similar abundances of these molecules at the beginning of the shock for both models (Figure 5). However, the abundance of PO is significantly enhanced not only during the collapse phase but, more importantly, in the post-shocked gas owing to the new formation route P + OH → PO + H. Figure 5 indeed shows that the PO abundance is enhanced by three orders of magnitude in the post-shocked gas (from a few 10^{-12} to a few 10^{-9}), thereby reaching values consistent with those measured in L1157-B1 (of $\sim 2.5 \times 10^{-9}$; see Lefloch et al. 2016). The enhancement of PO in the post-shocked gas is also possible thanks to the slight drop in the abundance of H₂O that increases the abundance of OH by several orders of magnitude when the temperature of the shocked gas reaches its maximum value (at about 50 yr after the passage of the shock; see also Jiménez-Serra et al. 2008). Note that the P + OH → PO + H reaction also seems to be the main mechanism responsible for the destruction of atomic phosphorus in the post-shocked gas (see blue lines in Figure 5). The predicted PO/PN ratios range between 3 and 9 in the post-shock region where PO is more abundant than PN (see Figure 5), which is also consistent with the observations (Lefloch et al. 2016; Rivilla et al. 2016, 2018, 2020; Bergner et al. 2019; Bernal et al. 2021).

5. Conclusions

In this paper, we have studied the formation route of the phosphorus monoxide (²PO) from the reaction of the oxygenated species H₂O and OH(²Π) with both the ground (⁴S) and the first metastable excited state (²P) of atomic P. Our theoretical results indicate that the formation of PO in the gas

⁵ Note that, in order to reproduce the measured abundances of PN and PO toward L1157-B1, atomic phosphorus needs to be depleted by a factor of 100 with respect to its solar value; otherwise, the abundances of these P-bearing species are overestimated (Aota & Aikawa 2012; Lefloch et al. 2016).

phase from the $P(^4S) + OH$ reaction is highly efficient because the rate-determining step of the whole process is the barrierless association reaction of the reactants. On the contrary, the first metastable excited state $P(^2P)$ should not react with OH under the same conditions due to a high energy barrier in the entrance channel. For the reaction of P with H_2O , the reactivity is reversed: while the reaction with $P(^4S)$ does not take place under the typical conditions of the ISM, that with $P(^2P)$ is highly efficient, being ruled by a rate-determining barrierless association. Overall, the reaction of atomic phosphorus in its ground state with OH is expected to be an important source of 2PO in the ISM because it enhances its abundance in shocked regions by several orders of magnitude. The modeled PO/PN ratios are indeed consistent with the values measured in the shocked gas associated with molecular outflows in star-forming regions.

This work has been supported by the Spanish State Research Agency (AEI) through project number MDM-2017-0737 Unidad de Excelencia “María de Maeztu”—Centro de Astrobiología (CSIC-INTA); by the MIUR “PRIN 2017” (grant No. 2017A4XRCA); by the Italian Space Agency (ASI; “Life in Space” project, N. 2019-3-U.0); by AEI (PID2019-105552RB-C41). I.J.-S. has received partial support from the Spanish State Research Agency (AEI; project number PID2019-105552RB-C41). Computational support was provided by the Super-computer facilities of LUSITANIA founded by Cénits and Computaex Foundation and by the SMART@SNS Laboratory (<http://smart.sns.it>).

Appendix

Cartesian coordinates (in angstroms) and harmonic frequencies (in cm^{-1}) of all stationary points

2PO

P 0.00000000 0.00000000 0.00000000
O 0.00000000 0.00000000 1.48500000
freq(harm) = 1223.74

2OH

O 0.00000000 0.00000000 0.00000000
H 0.00000000 0.00000000 0.97170000
freq(harm) = 3757.23

1PH

P 0.00000000 0.00000000 0.08887700
H 0.00000000 0.00000000 -1.33315100
freq(harm) = 2407.47

$^1TS_P-OH$

P 3.46948464 0.00000000 -0.30171826
O 0.00000000 0.00000000 0.98010000
H 0.00000000 0.00000000 0.00000000
freq(harm) = 3638.141 270.532 225.949i

1POH

P 1.50696687 0.00000000 1.57166368
O 0.00000000 0.00000000 0.96660000
H 0.00000000 0.00000000 0.00000000
freq(harm) = 3760.799 1070.214 894.533

3POH

P 1.50076273 0.00000000 1.63486360
O 0.00000000 0.00000000 0.96420000
H 0.00000000 0.00000000 0.00000000
freq(harm) = 3823.637933.103 827.148

(Continued)

$^1TS_POH-HPO$

P 0.00000000 0.00000000 1.52880000
O 1.18231570 0.00000000 0.41503159
H 0.00000000 0.00000000 0.00000000
freq(harm) = 2236.417 897.644 2010.099i

$^3TS_POH-HPO$

P 0.00000000 0.00000000 1.51110000
O 1.27629195 0.00000000 0.54335946
H 0.00000000 0.00000000 0.00000000
freq(harm) = 2134.077 944.020 1706.533i

1HPO

P 0.00000000 0.00000000 1.45680000
O 1.44309843 0.00000000 1.82608998
H 0.00000000 0.00000000 0.00000000
freq(harm) = 2169.554 1193.325 1008.357

3HPO

P 0.00000000 0.00000000 1.42860000
O 1.31934590 0.00000000 2.13424923
H 0.00000000 0.00000000 0.00000000
freq(harm) = 2248.498 1277.822 736.519

$^1TS_H-PO$

P 0.00000000 0.00000000 4.04900000
O 1.35434326 0.00000000 4.66632397
H 0.00000000 0.00000000 0.00000000
freq(harm) = 1199.271 88.235 512.679i

$^1TS_PO-H$

P 1.04552135 0.00000000 3.34359721
O 0.00000000 0.00000000 2.28130000
H 0.00000000 0.00000000 0.00000000
freq(harm) = 1233.134 363.761 394.336i

$^3TS_PO-H$

P 1.16667888 0.00000000 2.49535795
O 0.00000000 0.00000000 1.56920000
H 0.00000000 0.00000000 0.00000000
freq(harm) = 1286.444 484.534 2299.477i

H_2O

O 0.00000 0.00000 0.11772
H 0.00000 0.75970 -0.47088
H 0.00000 -0.75970 -0.47088
freq(harm) = 3938.962 3824.073 1644.853

$^2C_P-OH2$

P -0.82055 -0.00001 0.00804
O 1.15974 -0.00002 -0.09907
H 1.51540 -0.78402 0.33604
H 1.51487 0.78431 0.33591
freq(harm) = 3885.769 3772.303 1610.048 654.769 539.814 383.317

$^2TS_P-OH2$

P -0.75959 -0.02603 -0.00228
O 1.16713 0.01858 -0.11134
H 1.51114 -0.62345 0.52705
H 0.54567 0.86523 0.39787
freq(harm) = 3767.816 2110.363 940.039 822.651 637.448 1532.733i

2PHOH_anti

P -0.59530 -0.11409 -0.00000
O 1.04102 0.14268 0.00000
H 1.50919 -0.69911 0.00000
H -0.90777 1.26899 0.00000

(Continued)

freq(harm) = 3843.236 2407.780 1129.724 920.899 826.633 433.988

²TS_PHOH_rot

P 0.59726 -0.10260 0.01188

O -1.04704 0.02831 -0.11618

H -1.50635 0.02317 0.72984

H 0.92381 1.28946 0.02146

freq(harm) = 3842.659 2324.016 985.582 939.317 799.742 469.051i

²PHOH_syn

P 0.60247 -0.08676 -0.00000

O -1.04917 -0.09968 0.00001

H -1.45144 0.77374 0.00002

H 0.80776 1.32520 -0.00001

freq(harm) = 3862.082 2347.653 1086.997 908.622 819.464 305.855

²TS_PO-H2

P -0.53792 -0.13678 -0.00003

O 1.03330 -0.08189 0.00005

H 0.36012 1.17997 0.00003

H -0.55775 1.52688 -0.00002

freq(harm) = 2074.884 1895.574 1063.123 958.833 853.231 1924.571i

H₂

H 0.00000 0.00000 0.37110

H 0.00000 0.00000 -0.37110

freq(harm) = 2223.985

⁴C_P-OH2

P -1.47152 -0.00125 0.00437

O 2.10783 -0.00966 -0.06846

H 2.68106 -0.70795 0.25992

H 2.52906 0.80400 0.22228

freq(harm) = 3936.238 3821.003 1643.691 47.225 32.406 22.647

⁴TS_P-OH2

P 0.78930 -0.01662 -0.00002

O -1.03606 -0.00511 0.00003

H -1.34418 0.92132 0.00004

H -2.20681 -0.63113 0.00006

freq(harm) = 3639.759 1119.834 714.051 351.825 286.703 1854.174i

ORCID iDs

Juan García de la Concepción  <https://orcid.org/0000-0001-6484-9546>Cristina Puzzarini  <https://orcid.org/0000-0002-2395-8532>Vincenzo Barone  <https://orcid.org/0000-0001-6420-4107>Izaskun Jiménez-Serra  <https://orcid.org/0000-0003-4493-8714>Octavio Roncero  <https://orcid.org/0000-0002-8871-4846>

References

- Adler, T. B., Knizia, G., & Werner, H.-J. 2007, *JChPh*, **127**, 221106
- Alessandrini, S., Tonolo, F., & Puzzarini, C. 2021, *JChPh*, **154**, 054306
- Altwegg, B., Balsiger, H., Bar-Nun, A., et al. 2016, *SciA*, **2**, e1600285
- Andreazza, C. M., Almeida, A. A., & Borin, A. C. 2016, *MNRAS*, **457**, 3096
- Angeli, C., Cimiraaglia, R., Evangelisti, S., Leininger, T., & Malrieu, J.-P. 2001a, *JChPh*, **114**, 10252
- Angeli, C., Cimiraaglia, R., & Malrieu, J. 2001b, *CPL*, **350**, 297
- Aota, T., & Aikawa, Y. 2012, *ApJ*, **761**, 74
- Baiano, C., Lupi, J., Tasinato, N., Puzzarini, C., & Barone, V. 2020, *Molecules*, **25**, 2873
- Barone, V. 2004, *JChPh*, **120**, 3059

- Bergner, J. B., Öberg, K. I., Walker, S., et al. 2019, *ApJL*, **884**, L36
- Bernal, J. J., Koelemay, L. A., & Ziurys, L. M. 2021, *ApJ*, **906**, 55
- Bomble, Y. J., Vázquez, J., Kállay, M., et al. 2006, *JChPh*, **125**, 064108
- Charnley, S. B., & Millar, T. J. 1994, *MNRAS*, **270**, 570
- Chesnavich, W. J. 1986, *JChPh*, **84**, 2615
- Clyne, M. A. A., & Ono, Y. 1982, *JChSo, Faraday Trans.*, **2**, 1149
- Codella, C., Viti, S., Lefloch, B., et al. 2018, *MNRAS*, **474**, 5694C
- Cowan, R. D., & Griffin, M. 1976, *JOSA*, **66**, 1010
- Crehuet, R., & Bofill, J. M. 2005, *JChPh*, **122**, 234105
- Daranlot, J., Jorfi, M., Xie, C., et al. 2011, *Sci*, **334**, 1538
- Dionatos, O., Kristensen, L. E., Tafalla, M., Güdel, M., & Persson, M. 2020, *A&A*, **641**, A36
- Douglas, K. M., Blitz, M. A., Mangan, T. P., & Plane, J. M. C. 2019, *JPCA*, **123**, 9469
- Douglas, K. M., Blitz, M. A., Mangan, T. P., Western, C. M., & Plane, J. M. C. 2020, *JPCA*, **124**, 7911
- Dunning Jr., T. H. 1989, *JChPh*, **90**, 1007
- Dunning Jr., T. H., Peterson, K. A., & Wilson, A. K. 2001, *JChPh*, **114**, 9244
- Eckart, C. 1930, *PhRv*, **35**, 1303
- Fagerbakke, K. M., Sauval, A. J., Heldal, M., & Norland, S. 1996, *AME*, **10**, 15
- Feller, D. 1993, *JChPh*, **98**, 7059
- Fernández-García, C., Coggins, A. J., & Powner, M. W. 2017, *Life*, **7**, 31
- Francisco, J. S. 2003, *ChPh*, **287**, 303
- Frisch, M. J., Trucks, G. W., Schlegel, H. B., et al. 2016, Gaussian16, Revision C.01
- Georgievskii, Y., Miller, J. A., Burke, M. P., & Klippenstein, S. J. 2013, *JPCA*, **117**, 12146
- Grevesse, N., & Sauval, A. J. 1998, *SSR*, **85**, 161
- Grimme, S., Antony, J., Ehrlich, S., & Krieg, H. 2010, *JChPh*, **132**, 154104
- Grimme, S., Ehrlich, S., & Goerigk, L. 2011, *JCoCh*, **32**, 1456
- Gulick, A. 1957, *NYASA*, **69**, 309
- Handy, N. C., & Lee, A. M. 1996, *CPL*, **252**, 425
- Handy, N. C., Yamaguchi, Y., & Schaefer, H. F. 1986, *JChPh*, **84**, 4481
- Harding, M. E., Vázquez, J., Ruscic, B., et al. 2008, *JChPh*, **128**, 114111
- Helgaker, T., Klopper, W., Koch, H., & Noga, J. 1997, *JChPh*, **106**, 9639
- Henshaw, T. L., MacDonald, M. A., Stedman, D. H., & Coombe, R. D. 1987, *JPC*, **91**, 2838
- Holdship, J., Viti, S., Jiménez-Serra, I., et al. 2016, *MNRAS*, **463**, 802
- Holdship, J., Viti, S., Jiménez-Serra, I., Makrymallis, A., & Priestley, F. 2017, *AJ*, **154**, 38
- Husain, D., & Norris, P. E. 1977, *JChSo, Faraday Trans.*, **2**, 1107
- Husain, D., & Slater, N. K. H. 1978, *JChSo, Faraday Trans.*, **2**, 1627
- Jiménez-Serra, I., Caselli, P., Martín-Pintado, J., & Hartquist, T. W. 2008, *A&A*, **482**, 549
- Jiménez-Serra, I., Viti, S., Quénard, D., & Holdship, J. 2018, *ApJ*, **862**, 16
- Kállay, M., Nagy, P. R., Rolik, Z., et al. 2018, MRCC, A Quantum Chemical Program Suite, www.mrcc.hu
- Kállay, M., & Surján, P. R. 2001, *JChPh*, **115**, 2945
- Kendall, A., Dunning Jr., T. H., & Harrison, R. J. 1992, *JChPh*, **96**, 6796
- Knizia, G., Adler, T. B., & Werner, H.-J. 2009, *JChPh*, **130**, 054104
- Koo, B. C., Lee, Y. M., Moon, D. S., Yoon, S. C., & Raymond, J. C. 2013, *Sci*, **342**, 1346
- Kooij, D. M. 1893, *ZPhCh*, **12**, 155
- Kozuch, S., & Martin, J. M. L. 2011, *PCCP*, **13**, 20104
- Kutzelnigg, W. 1997, *MolPh*, **90**, 909
- Lee, T. J., & Taylor, P. R. 1989, *IQC*, **36**, 199
- Lefloch, B., Vastel, C., Viti, S., et al. 2016, *MNRAS*, **462**, 3937
- Lefloch, B., Vastel, C., Viti, S., et al. 2016, *MNRAS*, **462**, 3937
- Li, A., Xie, C., Xie, D., & Guo, H. 2011, *JChPh*, **134**, 194309
- Lupi, J., Puzzarini, C., & Barone, V. 2020, *ApJL*, **903**, L35
- Lupi, J., Puzzarini, C., Cavallotti, C., & Barone, V. 2020, *JCTC*, **16**, 5090
- Maciá, E. 2005, *CSR*, **34**, 691
- Martin, R. L. 1983, *JPC*, **87**, 750
- Mathews, D. A., Cheng, L., Harding, M. E., et al. 2020, *JChPh*, **152**, 214108
- McElroy, D., Walsh, C., Markwick, A. J., et al. 2013, *A&A*, **550**, A36
- Mininni, C., Fontani, F., Rivilla, V. M., et al. 2018, *MNRAS*, **476**, L39
- Neese, F., Wennmohs, F., Becker, U., & Riplinger, C. 2020, *JChPh*, **152**, 224108
- Nisini, B., Santangelo, G., Antonucci, S., et al. 2013, *A&A*, **549**, A16
- Noga, J., & Bartlett, R. J. 1987, *JChPh*, **86**, 7041
- Papajak, E., Leverentz, H. R., Zheng, J., & Truhlar, D. G. 2009, *JCTC*, **5**, 1197
- Pasek, M. A., & Laurretta, D. S. 2005, *AsBio*, **5**, 515
- Pechukas, P., & Light, J. C. 1965, *JChPh*, **42**, 3281
- Peterson, K. A., Adler, T. B., & Werner, H.-J. 2008, *JChPh*, **128**, 084102
- Peterson, K. A., & Dunning Jr., T. H. 2002, *JChPh*, **117**, 10548

- Prascher, B., Woon, D. E., Peterson, K. A., & Dunning Jr., T. H. 2011, *TCA*, 128, 69
- Puzzarini, C. 2006, *JMoSp*, 780, 238
- Puzzarini, C., & Barone, V. 2020, *PCCP*, 22, 6507
- Puzzarini, C., Salta, Z., Tassinato, N., et al. 2020, *MNRAS*, 496, 4298
- Rivilla, V. M., Drozdovskaya, M. N., Altwegg, K., et al. 2020, *MNRAS*, 492, 1180
- Rivilla, V. M., Fontani, F., Beltrán, M. T., et al. 2016, *ApJ*, 826, 161
- Rivilla, V. M., Jiménez-Serra, I., Zeng, S., et al. 2018, *MNRAS*, 475, L30
- Santra, G., Sylvetsky, N., & Martin, J. M. L. 2019, *JPCA*, 123, 5129
- Schwartz, A. W. 2006, *PTRSB*, 361, 1743
- Scuseria, G. E., & Schaefer III, H. F. 1988, *CPL*, 152, 382
- Sellers, H., & Pulay, P. 1984, *CPL*, 103, 463
- Stanton, J. F., Gauss, J., Harding, M. E., & Szalay, P. G. 2016, CFOUR. A Quantum Chemical Program Package, <http://www.cfour.de/>
- Suutarinen, A. N., Kristensen, L. E., Mottram, J. C., Fraser, H. J., & van Dishoeck, E. F. 2014, *MNRAS*, 440, 1844
- Tajti, A., Szalay, P. G., Császár, A. G., et al. 2004, *JChPh*, 121, 11599
- Tappe, A., Lada, C. J., Black, J. H., & Muench, A. A. 2008, *ApJL*, 680, L117
- Tonolo, F., Lupi, J., Puzzarini, C., & Barone, V. 2020, *ApJ*, 900, 85
- van Dishoeck, E. F., Herbst, E., & Neufeld, D. A. 2013, *ChRv*, 113, 9043
- van Dishoeck, E. F., Kristensen, L. E., Mottram, J. C., et al. 2021, *A&A*, 648, A24
- Vazart, F., Calderini, D., Puzzarini, C., Skouteris, D., & Barone, V. 2016, *JCTC*, 12, 5385
- Viti, S., Jiménez-Serra, I., Yates, J. A., et al. 2011, *ApJL*, 740, L3
- Viti, S., & Williams, D. A. 1999, *MNRAS*, 310, 517
- Wakelam, V., Loison, J.-C., Mereau, R., & Ruaud, M. 2017, *MolAs*, 6, 22
- Watts, J. D., & Bartlett, R. J. 1990, *JChPh*, 93, 6104
- Werner, H.-J., Knizia, G., & Manby, F. R. 2011, *MoPh*, 109, 407
- Werner, H.-J., Knowles, P. J., Knizia, G., et al. 2019, MOLPRO, v2019.2, A Package of Ab Initio Programs, <https://www.molpro.net/>
- Weston, R. E., & Schwartz, H. E. (ed.) 1972, Chemical Kinetics (Englewood Cliffs, NJ: Prentice-Hall Inc.)
- Woon, D. E., & Dunning, T. H., Jr. 1995, *JChPh*, 103, 4572
- Yamaguchi, V. M., Takano, S., Sakai, N., et al. 2011, *PASJ*, 63, L37